Immunobiology 225 (2020) 151863

Contents lists available at ScienceDirect

Immunobiology

journal homepage: www.elsevier.com/locate/imbio

Structural bases that underline *Trypanosoma cruzi* calreticulin proinfective, antiangiogenic and antitumor properties

Jaime Peña Álvarez[a,b,1], Jaime Teneb[b], Ismael Maldonado[b], Katherine Weinberger[b,2], Carlos Rosas[b,c,3], David Lemus[c], Carolina Valck[b], Álvaro Olivera-Nappa[a,4,*], Juan A. Asenjo[a,4,*], Arturo Ferreira[b,4,*]

[a] University of Chile, Faculty of Physical and Mathematical Sciences, CeBiB, Chile
[b] University of Chile, Faculty of Medicine, ICBM, Immunology Disciplinary Program, Chile
[c] University of Chile, Faculty of Medicine, Anatomy and Developmental Biology Disciplinary Program, ICBM, Experimental and Molecular Embryology Laboratory, Chile

ARTICLE INFO

Keywords:
Trypanosoma cruzi calreticulin
Complement
C1q
Tumor growth
Protein modeling
Molecular dynamics

ABSTRACT

Microbes have developed mechanisms to resist the host immune defenses and some elicit antitumor immune responses. About 6 million people are infected with *Trypanosoma cruzi*, the protozoan agent of Chagas' disease, the sixth neglected tropical disease worldwide. Eighty years ago, G. Roskin and N. Klyuyeva proposed that *T. cruzi* infection mediates an anti-cancer activity. This observation has been reproduced by several other laboratories, but no molecular basis has been proposed. We have shown that the highly pleiotropic chaperone calreticulin (TcCalr, formerly known as TcCRT), translocates from the parasite ER to the exterior, where it mediates infection. Similar to its human counterpart HuCALR (formerly known as HuCRT), TcCalr inhibits C1 in its capacity to initiate the classical pathway of complement activation. We have also proposed that TcCalr inhibits angiogenesis and it is a likely mediator of antitumor effects. We have generated several *in silico* structural TcCalr models to delimit a peptide (VC-TcCalr) at the TcCalr N-domain. Chemically synthesized VC-TcCalr did bind to C1q and was anti-angiogenic in *Gallus gallus* chorioallantoic membrane assays. These properties were associated with structural features, as determined *in silico*. VC-TcCalr, a strong dipole, interacts with charged proteins such as collagen-like tails and scavenger receptors. Comparatively, HuCALR has less polarity and spatial stability, probably due to at least substitutions of Gln for Gly, Arg for Lys, Arg for Asp and Ser for Arg that hinder protein-protein interactions. These differences can explain, at least in part, how TcCalr inhibits the complement activation pathway and has higher efficiency as an antiangiogenic and antitumor agent than HuCALR.

1. Introduction

Pathogens have evolved to resist the host immune response by several mechanisms. In apparently unrelated ways, some pathogens inhibit cancer progression at its hosts (Baird et al., 2013; Chen et al., 2011; Hunter et al., 2001; Noya et al., 2013; Oikonomopoulou et al., 2014; Oliveira et al., 2001; Plumelle et al., 1997; Ubillos et al., 2016; van Tong et al., 2017). Although these antitumor effects were reported several decades ago for a variety of aggressors, information on pathogen molecules involved and their biochemical mechanisms has been limited (López et al., 2010; Ramírez-Toloza et al., 2016).

Trypanosoma cruzi anticancer activity was proposed 80 years ago (Camidge and Krementsov, 2002; Klyuyeva and Roskin, 1963; Krementsov, 2009; Roskin and Exempliarskaia, 1931; Roskin, 1946). About 5.7 million people in 21 endemic countries are infected with this parasite and near 30% manifest the chronic phase of Chagas' disease, a worldwide neglected reemerging tropical illness (Coura and Viñas, 2010; Pérez-Molina et al., 2015; World Health Organization, 2015). It was formerly endemic in rural and peri urban areas throughout Latin America, where *Hemiptera* insects of the subfamily *Triatominae*

* Corresponding authors.
E-mail addresses: aolivera@ing.uchile.cl (Á. Olivera-Nappa), juasenjo@ing.uchile.cl (J.A. Asenjo), aferreir@med.uchile.cl (A. Ferreira).
[1] Present address: Universidad Autónoma de Chile, Facultad de Ingeniería, Ingeniería Civil Industrial, Chile.
[2] Present address: Universidad San Sebastián, Facultad de Medicina y Ciencia, Departamento de Ciencias Morfológicas, Chile; Universidad Mayor, Facultad de Ciencias, Escuela de Medicina Veterinaria, Chile.
[3] Present address: Universidad San Sebastián, Facultad de Medicina y Ciencia, Departamento de Ciencias Morfológicas, Chile.
[4] They contributed equally to this research.

https://doi.org/10.1016/j.imbio.2019.10.012
Received 26 October 2019; Accepted 29 October 2019
Available online 05 November 2019
0171-2985/

(Reduviidae), that reside in crevices of the walls/roofs of poorly constructed houses, transmit the parasite after sucking blood at night and defecating. The parasite enters to the bloodstream when a person comes in contact with parasite-contaminated feces/urine through a break in the skin (including the bite), eyes or mouth. In areas with intra-domiciliary vector transmission, typically children that are less than 5 years old are infected (World Health Organization, 2015). However, Chagas' disease has gone global due to migrations to USA, Canada, Europe, Oceania, and Asia (Tanowitz et al., 2011). Transmission is mainly by blood transfusions, organ transplants, contaminated foods or congenital (Coura, 2006; Flores-Chávez et al., 2008; Freilij and Altcheh, 1995; Kun et al., 2009; Ramírez-Toloza et al., 2014; Sosoniuk et al., 2014; Yoshida, 2009).

Several *T. cruzi* strains display growth inhibitory effects over multiple transplanted and spontaneous tumors in animal models and humans (Kallinikova et al., 2001; Oliveira et al., 2001). This property has been attributed to a "toxic substance" excreted by the parasite that reduced pain, tumor growth, bleeding and local inflammation (Klyuyeva and Roskin, 1963; Krementsov, 2009; Roskin, 1946). Also, chronically infected rats are more resistant to 1,2-dimethylhidrazyne-induced carcinoma (Oliveira et al., 2001), and the parasite displays tropism for tumor cells, suggesting an antagonistic relationship between Chagas' disease and cancer development (Kallinikova et al., 2001). Elemental Darwinian reasoning allows suggesting that the parasite survival would prevail only if host survival is assured.

In response to these hypotheses, tumor growth inhibition by tumor/parasite competition for nutrients has been proposed (Hauschka and Goodwin, 1948; Malisoff, 1947). This proposal is not entirely satisfactory, since tumors develop their own blood vessels through angioneogenesis in order to obtain nutrients and oxygen, and to remove wastes (Folkman, 2003), and their growth may drain the available nutrients, leading their hosts to advanced cachexia stages. On the other hand, the activation of T cell-mediated immunity using a recombinant non-pathogenic *T. cruzi* clone as a vector of a testis tumor antigen delayed tumor development in infected mice (Junqueira et al., 2011), thus strengthening the "toxic substance" hypothesis. Other laboratories have corroborated the antitumor effect of *T. cruzi* infection in different animal models (Atayde et al., 2008; Cabral, 2000; Junqueira et al., 2012; Kallinikova et al., 2001; Mel'nikov et al., 2004; Oliveira et al., 2001; Sheklakova et al., 2003; Ubillos et al., 2016; Zenina et al., 2008). Current information indicates that, most likely, several parasite molecules and mechanisms are involved in the tumor resistance mediated by *T. cruzi* infection.

In our laboratory, a *T. cruzi* gene coding for a 45 kDa protein was cloned, sequenced and expressed. It shares 60% similarity and 42% identity with human calreticulin (HuCALR, formerly known as HuCRT), a multifunctional constitutive ER-resident chaperone (Michalak et al., 2009).

We identified this protein in *T. cruzi* and first called it Tc45 (Ramos et al., 1991), then TcCRT (Aguillón et al., 2000; Ferreira et al., 2004a, 2002) and now it is known as TcCalr. Like HuCALR (Stuart et al., 1997, 1996), TcCalr *in vitro* inhibits the classical pathway of human complement activation, an important arm of the innate and adaptive immune responses, inactivating C1 (Ferreira et al., 2005, 2004b, 2004a) and interfering with the serine proteases $(C1r–C1s)_2$ activation of the complement component C4, as a likely immune evasion strategy (Valck et al., 2010). Also, TcCalr operationally interferes with C1s activity in a calcium-independent manner, without involving the release of the protease from the C1q recognition molecule (Valck et al., 2010). Moreover, TcCalr is translocated from the ER to the area of flagellum emergence in trypomastigotes, the *T. cruzi* infective form in mammal hosts. Most likely, *in vivo*, the parasite recruits C1 and inhibits complement. C1, still bound to the parasite surface, is recognized by cC1qR (a membrane form of mammal calreticulin) and parasitic infectivity is significantly enhanced (reviewed by Ramírez-Toloza et al., 2016).

Complement strategies to inhibit the immune response are not unique to parasites such as *T. cruzi*. We have proposed that its hematophagous arthropod vector, *Triatoma infestans*, also inhibits this innate immune defense by using its salivary calreticulin to inactivate the complement present in its blood meal, thus preventing damage to the insect intestinal mucosa (Weinberger et al., 2017).

Complement inhibition and increased infectivity, two central events in host/parasite interactions, are evident (Ferreira et al., 2004b; Rimoldi et al., 1989). This extraordinary TcCalr pleiotropism is even reflected in its capacity to interact with endothelial cells and inhibit both angiogenesis and tumor growth (López et al., 2010; Ramírez et al., 2011). Most importantly, these effects are reversed by anti-TcCalr F $(ab')_2$ bivalent IgG fragments, in *T. cruzi* infection, and by anti-TcCalr whole IgG in *T. cruzi* epimastigotes (non-infective form) extract administration (Abello-Cáceres et al., 2016). These findings identify TcCalr as responsible for at least an important part of the antitumor effects observed in *T. cruzi* infection.

Some authors have proposed that whole HuCALR, and fragments thereof, are antiangiogenic and have potential for antitumor therapies. They identified the HuCALR N-terminal polypeptides encompassing residues 1-180 (vasostatin) (Pike et al., 1998), 120-180 (120-180, named here as VL-HuCALR) (Pike et al., 1999) (both numberings do not take into account HuCALR N-terminal signal sequence) and 135-164 (an active fragment of vasostatin, named here as VC-HuCALR, that does account for the HuCALR N-terminal signal sequence) (Li et al., 2007), as promising candidates.

Herein, we have delimited *in silico* one main fragment, at the TcCalr N-domain, that mediates significant proportion of the antiangiogenic and antitumor properties observed in the whole protein. This TcCalr peptide, encompassing residues 131-159, named here as VC-TcCalr, similar to VC-HuCALR. VC-TcCalr activity was assessed *in vitro* by the capacity of solid phase bound TcCalr and peptides, to interact with C1q. Also, this activity was measured *in ovum* in the *Gallus gallus* chick embryonic chorioallantoic membrane (CAM) assay.

Structural bioinformatic analysis revealed the strong dipole nature of VC-TcCalr that enables the interaction with charged proteins such as collagen-like tails and scavenger receptors. When compared both whole TcCalr and HuCALR, the human counterpart displayed less polarity and spatial stability than the protozoan orthologue, probably due to specific amino acidic substitutions that hinder protein-protein interactions. These differences seem to explain, at least to some extent, the molecular mechanisms describing how TcCalr inhibits complement, evidencing higher efficiency in its antiangiogenic and antitumor properties than HuCALR.

2. Materials and methods

2.1. TcCalr and HuCALR sequence alignment

Amino acid sequences of whole TcCalr (Aguillón et al., 2000) and HuCALR (Lamerdin et al., 1996) were retrieved from the National Center for Biotechnology Information website (www.ncbi.nlm.nih.gov) (GenBank: AAD45370 and AAB51176 respectively). These sequences were aligned with the Clustal Omega v1.2.1 Multiple Sequence Alignment program (www.ebi.ac.uk/Tools/msa/clustalo), job id: clustalo-E20150424-193624-0275-39009658-oy (Sievers et al., 2011).

2.2. TcCalr in silico modeling and protein visualization

Since TcCalr three-dimensional structures were not available at the start of this work, it was *in silico* modelled using the Robetta Full-chain Protein Structure Prediction Server (www.robetta.org) (Kim et al., 2004). To assess the overall stereo chemical quality of the model, the SWISS-MODEL server (swissmodel.expasy.org) (Biasini et al., 2014) uses several tests: QMEAN (Benkert et al., 2009a), ANOLEA (Melo and Feytmans, 2008), GROMOS (van Gunsteren et al., 1996), DFire (Zhou and Zhou, 2002) and Ramachandran plot (Ramachandran et al., 1963).

```
HuCALR      MLLSVPLLLGLLGLAVAEPAVYFKEQFLDGDGWTSRWIESKHKSDFGKFVLSSGKFYGDEEK 62
TcCalr      AAIFFCALLGLATLSAVHGTVYFHEEFKSME----HWTTSKHRDDFGKVEISAGKFYADAEK 58
              : .  **** *:... :***:*:* . :    :*  ***:.****. :*:****.* **

HuCALR      DKGLQTSQDARFYALSASFE-PFSNKGQTLVVQFTVKHEQNIDCGGGYVKLFPNSLDQTDMH 123
TcCalr      SKGLRLTEDARFYALSTAFPTPITNEKKSLVVSFSVKHEQDLKCGGGYIKLLPS-MDPEKFH 119
            .***: ::********::*  *::*: ::***.*:*****::.*****:**:*. :*  .:*

HuCALR      GDSEYNIMFGPDICGPGTKKVHVIFNYKGKNVLINKDIRCKDDEFTHLYTLIVRPDNTYEVK 185
TcCalr      GETKYWLVFGPDRCGSQ-NRVHIILHYNGENREWSKRISFPEDKLTHVYTLHIAADNSYEFF 180
            *:::* ::**** **   ::**:*:.*:*:*   .* *   :*::**:*** :  **:**.

HuCALR      IDNSQVESGSLEDDWDFLPPKKIKDPDASKPEDWDERAKIDDPTDSKPEDWDK-PEHIPDPD 246
TcCalr      LDGESKAKGQLEEDWSLLLPREIVDETDKKPEDWVDEETMDDPEDKKPEDWDNEPAMIPDPD 242
            :* ..  .*.**:**.:* *::* *   .***** :. .:*** *.******: *  *****

HuCALR      AKKPEDWDEEMDGEWEPPVIQNPEYKGEWK-----PRQIDNPDYKGTWIHPEIDNPEYSPDP 303
TcCalr      AKKPDDWDDAEDGPWEAPMIRTRSRKAHGSHVKFPTRRTRACGSRGRFLIQN-----FVEDS 299
            ****:***:  ** ** *:*:. . *.. .      *:      :* ::  :     :  *

HuCALR      -SIYAYDNFGVLGLDLWQVKSGTIFDNFLITNDEAYAEEFGNETWGVTKAAEK----QMKDK 364
TcCalr      ELHKVREPLTHVGIDVWQVESRSIFKDIVIGDDLKEVLDLVEKTYGRPEEGGGGSLKVMEDM 361
                . : :  :*:*:***:* :**.:::* :*   . :: ::*:*  : .       *:*

HuCALR      QDEEQRLKEEEEDKKRKEEEEAEDKEDDEDKDEDEEDEEDKEEDEEEDVPGQAKDEL 417
TcCalr      EK-EKRKKEEEEEREKEKEKPEEEKV--------EEELEKKGDRDKEDL-------- 401
            :. *:* *****::::::*:  *:*         **: *.* : ::**:
```

Fig. 1. Structural sequence alignment of HuCALR and TcCalr. Underlined residues correspond to the S. Pike group's 120-180 Cal sequence (Pike et al., 1999) and its parasitic similar VL-TcCalr, and overlined ones to the X. Li group's active fragment of vasostatin (N-terminal aa 135-164 of HuCALR) (Li et al., 2007) and its parasitic similar VC-TcCalr. The alignment was performed by Clustal Omega v1.2.1 Multiple Sequence Alignment program (www.ebi.ac.uk/Tools/msa/clustalo), job id: clustalo-E20150424-193624-0275-39009658-oy (Sievers et al., 2011).

All models were visualized in VMD (Humphrey et al., 1996) and PyMOL (DeLano, 2002).

2.3. Molecular dynamics, electrostatic potential and field simulations

Models were protonated at the H++ server (biophysics.cs.vt.edu) (Anandakrishnan et al., 2012; Gordon et al., 2005) in mammal blood conditions: 310 K, pH 7.4, 0.15 mol/l NaCl, internal dielectric constant of 10 and external dielectric constant of 80. Molecular dynamics (MD) simulations were performed locally and remotely at Leftraru supercomputer, located at the National Laboratory for High Performance Computing (NLHPC), Center for Mathematical Modeling (CMM), University of Chile (www.nlhpc.cl), using the NAMD2 package with AMBER force field parameters with an NVT ensemble, constant temperature of 310 K and a 2 fs timestep (Kalé et al., 1999; Phillips et al., 2005; Wang et al., 2004). Root Mean Square Deviation (RMSD) scripts and electrostatic simulations were performed by Adaptive Poisson-Boltzmann Solver server (APBS) (Baker et al., 2001; Holst and Saied, 1993) aided by the PDB2PQR package (Dolinsky et al., 2007, 2004) (www.poissonboltzmann.org). MD simulations, electrostatic potentials and fields were visualized in VMD (Humphrey et al., 1996).

2.4. rTcCalr, VC-TcCalr and VC-HuCALR binding to C1q

C1q-binding protein and peptides were assessed by ELISA with modifications (Ferreira et al., 2004b). Plastic microtitration plates (Nunc MaxiSorp, USA) were sensitized with 100 µl/well of rTcCalr (1.28 µM), VC-TcCalr, VC-HuCALR and scrambled VC-TcCalr (all at 2.56 µM) diluted in carbonate buffer (15 mM Na_3CO_3, 35 mM $NaHCO_3$, pH 9.6), overnight at 4 °C. After blocking the remaining active sites with 200 µl/well of PBS/BSA 3% for 2 h at 37 °C, and washed four times with 250 µl/well of PBS/Tween-20 (PBS supplemented with 0.05% Tween-20), C1q (0, 1 and 2 µg/ml from Sigma-Aldrich, in Veronal buffer, VB^{2+} (5,5-diethylbarbituric acid sodium salt 5 mM, NaCl 140 mM, $MgCl_2$ 0.5 mM, $CaCl_2$ 0.15 mM, 0.05% v/v Tween-20)) was added. After 1 h at 37 °C and washing, binding was measured using goat polyclonal anti-C1q antibodies (Sigma-Aldrich, USA), and detected with a rabbit polyclonal anti-goat peroxidase-bound IgG as secondary antibody and ABTS as substrate (Calbiochem, USA). The reactions were read at 405 nm. Recombinant TcCalr (rTcCalr) was generated at our laboratory (Ferreira et al., 2004b), and VC-TcCalr and VC-HuCALR were chemically synthesized at Curauma Biotechnology Nexus, Santiago, Chile. Human C1q was obtained from Complement Technology, Tyler, TX, USA. Scrambled VC-TcCalr and C1q solvent were used as negative controls.

2.5. Chick embryonic chorioallantoic membrane assay

The chick embryonic chorioallantoic membrane (CAM) assay was performed as previously described (Lemus et al., 2001; Molina et al., 2005; Xiao et al., 2002; Zúñiga et al., 2003). Briefly, 48 fertilized White Leghorn hen eggs (National Public Health Institute, Santiago, Chile) were used in protein and peptide assays, where 12 eggs per condition were alternatively instilled with 1.517 ng of VC-TcCalr, 10 ng of rTcCalr as positive control, 1.517 ng of scrambled VC-TcCalr and 738.5 ng BSA diluted in PBS prepared with endotoxin-free bidistilled water, as negative controls. The eggs were incubated for 48 h in a humid 38.5 °C atmosphere. After extracting 2–3 ml of albumin, a small window was opened in the egg, in order to allow separation of the CAM from the shell during the embryo development. The window was temporarily sealed with adherent tape and the eggs were incubated for additional 5 days. Then, sterile methyl cellulose discs (5 mm diameter, 0.25 µm pore size, 125 µm thickness) (Advantec MFS Inc., CA, USA), were deposited on the CAMs. Immediately, 10 µl of each sample were directly added onto the filters. The windows were then sealed, and the eggs were incubated for additional 72 h, as indicated above. Then, CAMs were sliced following the filters contours and fixed in 10% (v/v) formaldehyde. Tissue sections were prepared by standard procedures for conventional light microscopy aimed at detecting mainly acid polysaccharides, nuclei and cytoskeleton. Blood vessels were counted in a light microscope with a 1 cm^2 micrometric grid, divided in 1 mm^2 sections. Ten of these sections, corresponding to a tissue area of 9000 μm^2 were counted. Blood vessels were identified mainly by their endothelial cells and by the presence of red blood cells in their lumens. Counting, carried out in a double-blind fashion, was performed in 29 microscopic fields of CAM tissue segments, adjacent to the filter edge.

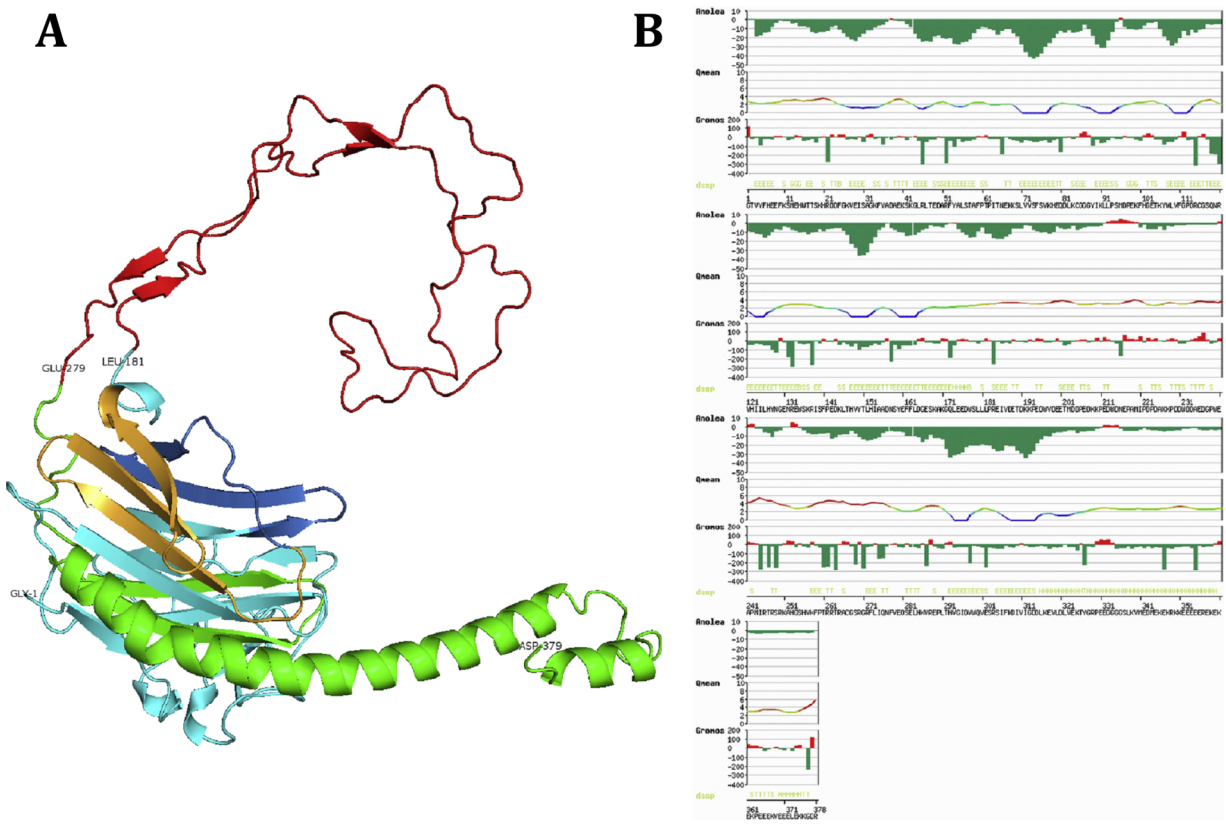

Fig. 2. (A) TcCalr-SS-KEDL-ROBETTA_1, best TcCalr*in silico* model. TcCalr N-domain, VC-TcCalr, VL-TcCalr, P domain and C-domain are depicted in cyan, sky blue, sky blue-bright orange, red and green respectively. Labeled residues are domain boundaries. Signal and destiny sequences were removed. (B) TcCalr-SS-KEDL-ROBETTA_1 ANOLEA, QMEAN and GROMOS structure quality reports (Biasini et al., 2014). (For interpretation of the references to colour in the figure legend and text, the reader is referred to the web version of this article.)

3. Results

3.1. TcCalr in silico modeling

The aminoacidic sequence of HuCALR (Li et al., 2007; Pike et al., 1999, 1998) was aligned with that of TcCalr in order to find similar sectors in both proteins (Fig. 1). We focused on HuCALR fragments delimited by residues 120-180 and 135-164 (VL-HuCALR and VC-HuCALR, according to Pike's and Li's numbering, respectively). For this purpose, the latter sequence is also identified here as the "vasostatin-like zone". Their corresponding sequences in the parasite chaperone are VL-TcCalr, encompassing residues 131–192, 39% identical and 57% similar to VL-HuCALR, and VC-TcCalr, encompassing residues 131–159, 38% identical and 59% similar to VC-HuCALR.

Then, the VL-TcCalr, VC-TcCalr, TcCalr and HuCALR peptide models were compared. Only a partial HuCALR crystallographic model was available when we started these studies, composed mainly by its globular domain (PDB IDs 3POW and 3POS) (Chouquet et al., 2011), a detailed TcCalr protein model was not available. Among the several *in silico* models generated, the best one, TcCalr-SS-KEDL-ROBETTA_1 (Fig. 2, left), was obtained from the Robetta Full-chain Protein Structure Prediction Server (www.robetta.org) (Kim et al., 2004), using its primary sequence without its signal and destiny sequences and PDB ID 3RG0 *Mus musculus* calreticulin chain A as template (Pocanschi et al., 2011). The model obtained clearly resembles the 3D structure of 3RG0. Then, its quality was assessed by SWISS-MODEL Structure Assessment Tools (swissmodel.expasy.org) (Biasini et al., 2014). Its extensive ANOLEA and GROMOS favorable energy zones (Fig. 2, right, depicted in green) (Melo and Feytmans, 2008; van Gunsteren et al., 1996), raw and absolute (Z) QMEAN6 scores (0.698/-0.838) (Benkert et al., 2011, 2009a, b), Ramachandran plot values of 85% of core, 13.5% of allowed regions, 0.9% in general and 0.6% in disallowed regions (Ramachandran et al., 1963), and DFire energy (−471.52) (Zhou and Zhou, 2002) match with values of native and well-folded proteins. Therefore, they are very acceptable for further analysis.

3.2. Molecular dynamics

The TcCalr and HuCALR structures were placed in a physiological simulated media in order to model a human blood-like environment *in silico* and to simulate their dynamic behavior. As globular domain dynamics usually require shorter execution times to achieve structural equilibrium, TcCalr middle P and terminal C domains were removed in the same way as in 3POW-3POS HuCALR crystallographic structures. Fig. 3A depicts a TcCalr globular domain (GCG-TcCalr) before molecular dynamics (MD), Fig. 3B shows GCG-TcCalr after MD and Fig. 3C illustrates a VC-TcCalr model after MD. Fig. 3D represents a 3POS HuCALR model after MD for comparison with other simulations. Simulation parameters for the models in Figs. 3B, C and D were a theoretical simulated time of 60/30/60 ns, a time for structural equilibration of 41/22/45 ns, and amino acid Root Mean Square Deviation (RMSD) relative to the beginning of the simulations of 3.25/4.25/2.25 Å, with a variation of 0.65/0.5/0.5 Å, respectively. These values match the ones of native structures, since the maximum RMSD is lower than 6 Å (Reva et al., 1998).

A study of hydrogen bond interactions within the globular domains at the vasostatin-like zone was performed using the *HBonds* representation in VMD. A 2.8/3.5 Å distance was considered for mild/weak hydrogen bonds, respectively. In Fig. 4, VC-TcCalr (A) and VC-HuCALR (B) characteristic hydrogen bond motifs are shown.

VC-TcCalr (Fig. 4A) has two particular zones: the coils at the N- and C-terminal ends, called here "start/end coils" and a two-strand beta-

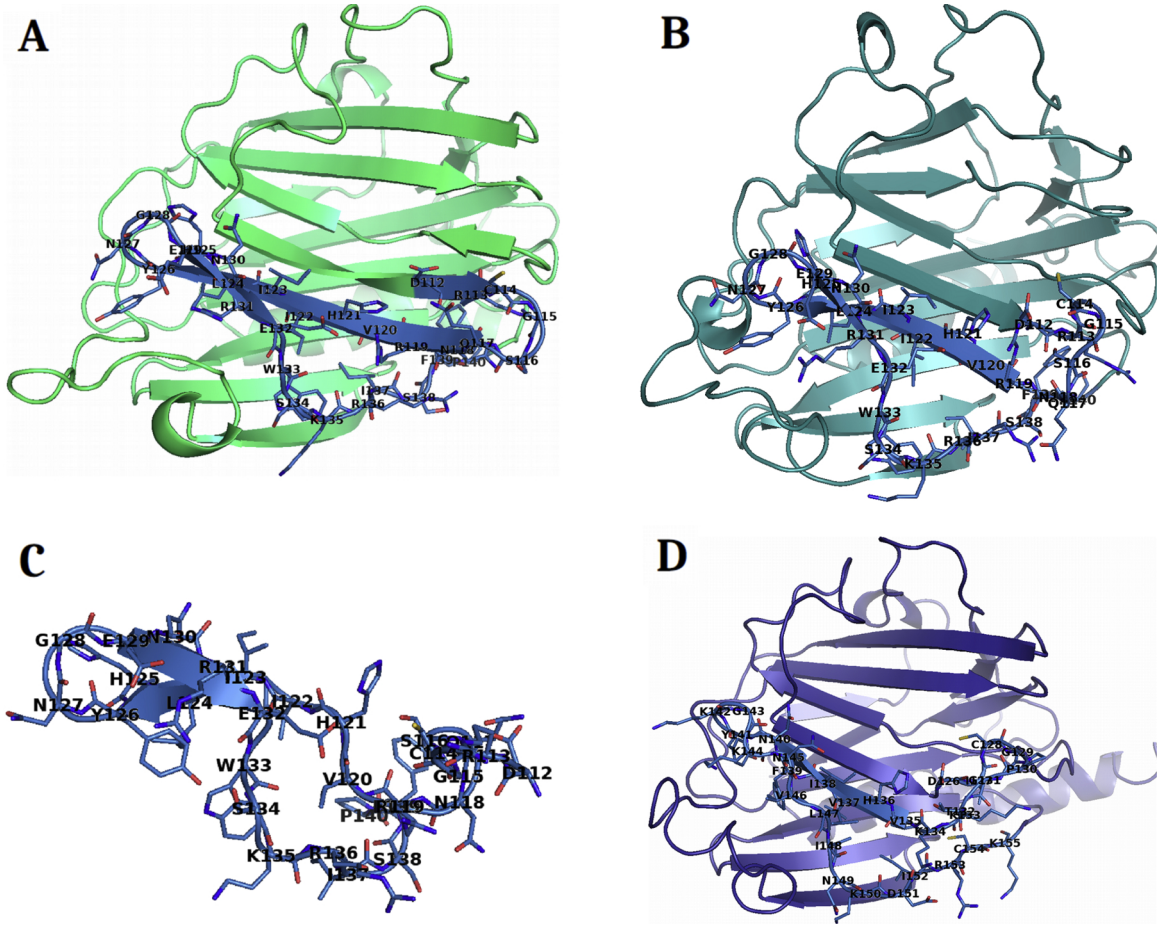

Fig. 3. *In silico* models before and after molecular dynamic simulations. (A) GCG-TcCalr-SS-C_KEDL_ROBETTA_SWISS_H, before MD (light green). (B) GCG-TcCalr-SS-C_KEDL_ROBETTA_SWISS_H_postMD (deep teal). (C) VC-TcCalr-SS-C_KEDL_ROBETTA_SWISS_H_postMD (sky blue). (D) HuCALR-3POS_SWISS_H-postMD (deep blue) (Pike et al., 1999). In all models, VC-TcCalr zone is depicted with sticks in sky blue (Biasini et al., 2014; DeLano, 2002; Humphrey et al., 1996; Kalé et al., 1999; Kim et al., 2004; Phillips et al., 2005). (For interpretation of the references to colour in the figure legend, the reader is referred to the web version of this article.)

sheet with a beta-turn between both strands, formed by the central residues. Start/end coils possess a rich hydrogen bond network, giving this zone a mainly rigid mechanics. The same applies for the beta-turn since R, H and E residues form saline bridges, and Y126 and R131 are involved in a cation-pi interaction. Therefore, VC-TcCalr has two interacting sectors structures that stabilize this zone.

In contrast, VC-HuCALR has a more disorganized and elastic hydrogen bond network, (Fig. 4B). R119 is replaced by K134, somewhat less efficient to form saline bridges, R136 by D151, changing its polarity, Q117 (medium size) by G131 (small size) and S138 (neutral) by R153 (positive). Particularly, R153 interactions modify charges, stability and shape of the start/end coils. In addition, several residues at the concave side of its central beta strand have a non-polar nature (R, E change to V, L), weakening the dipole behavior observed at VC-TcCalr and making VC-HuCALR less able to interact with charged molecules. Therefore, and in opposition with VC-TcCalr (more rigid and dipolar), VC-HuCALR is more flexible and non-polar, more suitable to adapt to several environments, as required for a good chaperone function.

The electrostatic potential and field of the vasostatin-like zone in both parasite and human ortholog proteins were studied to analyze electrostatic and solvation properties that allow whole calreticulins to interact with other charged proteins. In Fig. 5A, the GCG-TcCalr

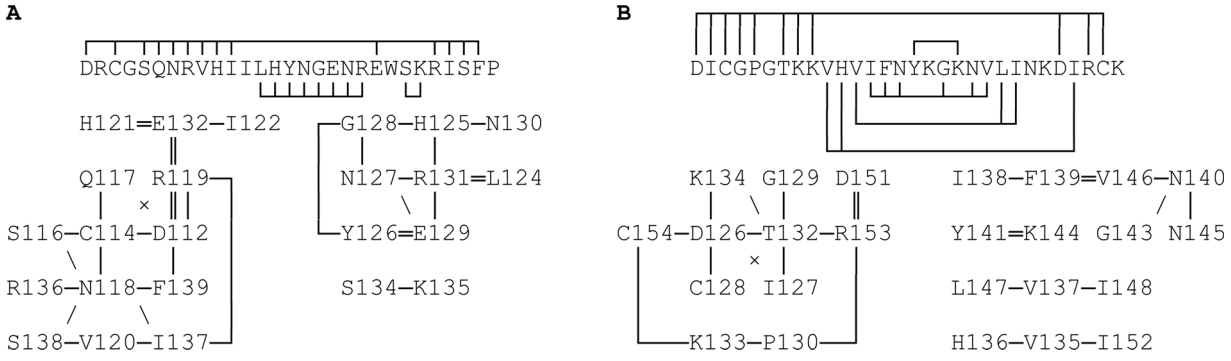

Fig. 4. Hydrogen bond network within the vasostatin zone at Calr globular domains in (A) VC-TcCalr network and (B) VC-HuCALR. Dashes between residues represent the number of hydrogen bonds established.

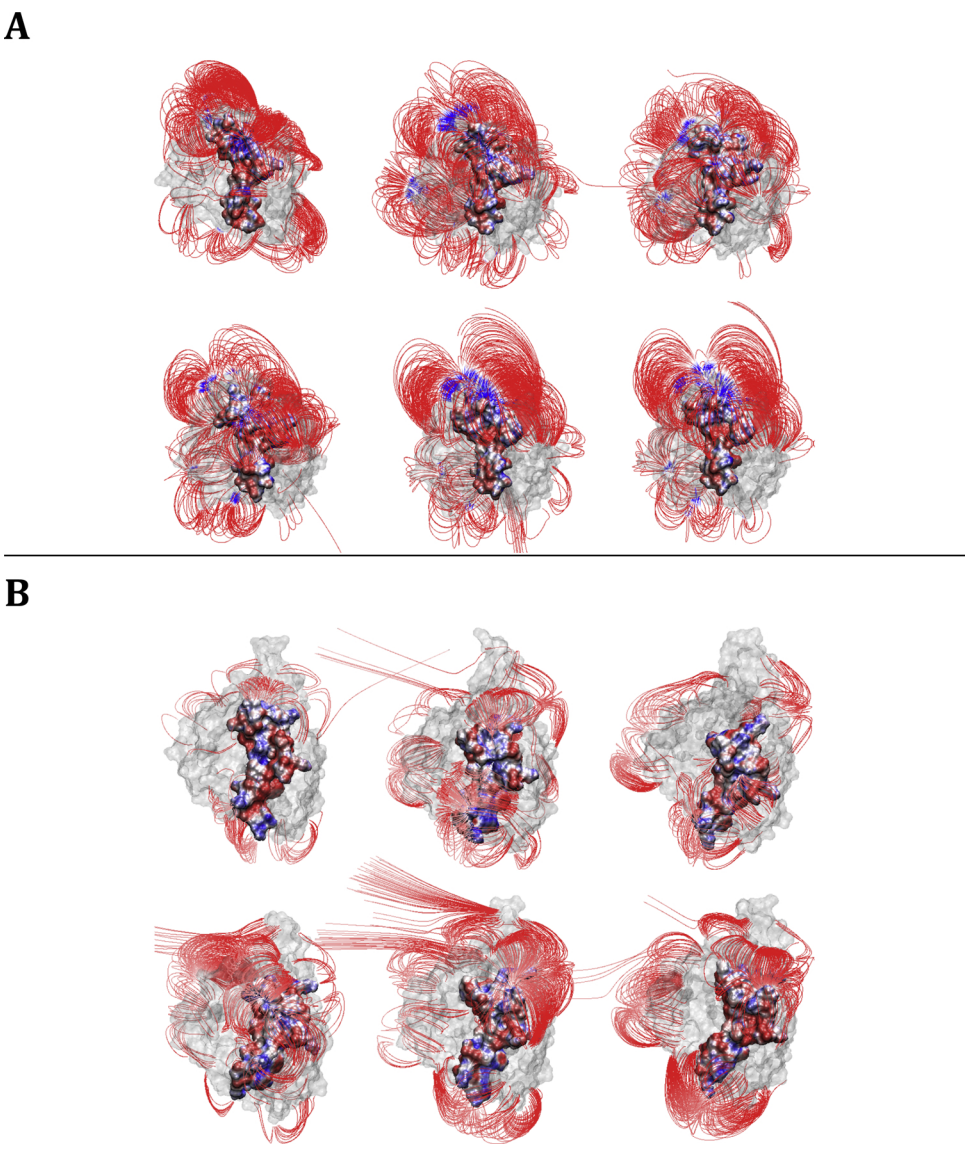

Fig. 5. Electrostatic potential and field of A) GCG-TcCalr and B) HuCALR-3POS during molecular dynamics simulations. For each 6-frames group, from left to right and up to down, first frames represent the initial protein model, the next four the productive phase models and the last ones their resulting configuration. Positive, neutral and negative electrostatic regions are depicted in blue, white and red respectively. The remaining protein is represented in a light-gray background. Molecular dynamics were performed with NAMD2 (www.ks.uiuc.edu/Research/namd), the maps were elaborated at APBS & PDB2PQR website (www.poissonboltzmann.org) and the proteins were depicted with VMD suite (www.ks.uiuc.edu/Research/vmd) (DeLano, 2002). (For interpretation of the references to colour in the figure legend and text, the reader is referred to the web version of this article.)

electrostatic potential (surface depiction) shows a positive (blue) region at start/end coils, negative (red) region at the beta-turn and a negative recess at the concave side in the central beta-sheet. This is also seen in Fig. 3A, B, C, where several non-polar residues (V, I, L) have their sidechains facing the convex side of the TcCalr globular domain thus forming the negative recess. Other polar or charged sidechains (N, R, H, E) facing the concave side form a positive groove, thus imparting VC-TcCalr a dipolar nature. In addition, the electrostatic field lines are directed towards the start/end coils (negative to positive sense), suggesting a central role in binding to other molecules, and its spatial distribution is mainly conserved, making it more appropriate to bind charged rigid molecules like C1q collagenous tails or scavenger receptors with collagenous domains.

On the other hand, in Fig. 5B the 3POS electrostatic potential shows more neutral start/end coils, a more positive beta-sheet turn and mixed charges in beta-strands. In contrast to GCG-TcCalr, its electrostatic field is less directed towards the start/end coils and more to the beta-turn, which could indicate that both regions are equally relevant in the protein. The spatial distribution is less conserved, suggesting more varied interactions and also supporting the more marked chaperone activity of this protein, as stated above. Thus, GCG-TcCalr is more polar than 3POS, its field flow is mainly opposite, and its binding properties are different, which probably supports its particular antiangiogenic and antitumor properties.

3.3. Comparison of TcCalr and HuCALR binding/active sites

Once TcCalr and HuCALR structural information after MD was obtained, it was possible to analyze in more detail their binding/active sites in order to propose binding mechanisms with other molecules.

A crystallographic structure of TcCalr has been solved based on 3POW and 3POS guidelines (PDB ID 5HCF; Moreau et al., 2016), in which a lectin binding surface with a hollow structure is formed by 5 G and 1 P at the concave face of the molecule and a glucose molecule is bound within. This is common for calreticulins and calnexins, which are also quality-control molecular chaperones that reside in the ER (Chouquet et al., 2011; Kozlov et al., 2010; Schrag et al., 2001). On this surface, binding subsites for glucose (GBS) and peptides (PBS) are found, not shaped as pockets but including hydrophobic residues relevant for binding. The GBS is more conserved between species, mainly in its M, I, K, Y (and less important G and D) residues, while the PBS includes a disulfide bridge, a W at the edge of the lectin site, D, H, S, F, V and other hydrophobic residues forming polar and *van der Waals* interactions. Our group has proposed that calreticulin genes are particularly prone to evolutionary pressures, given the relevance of the biological functions that these molecules must satisfy. Since the subsites

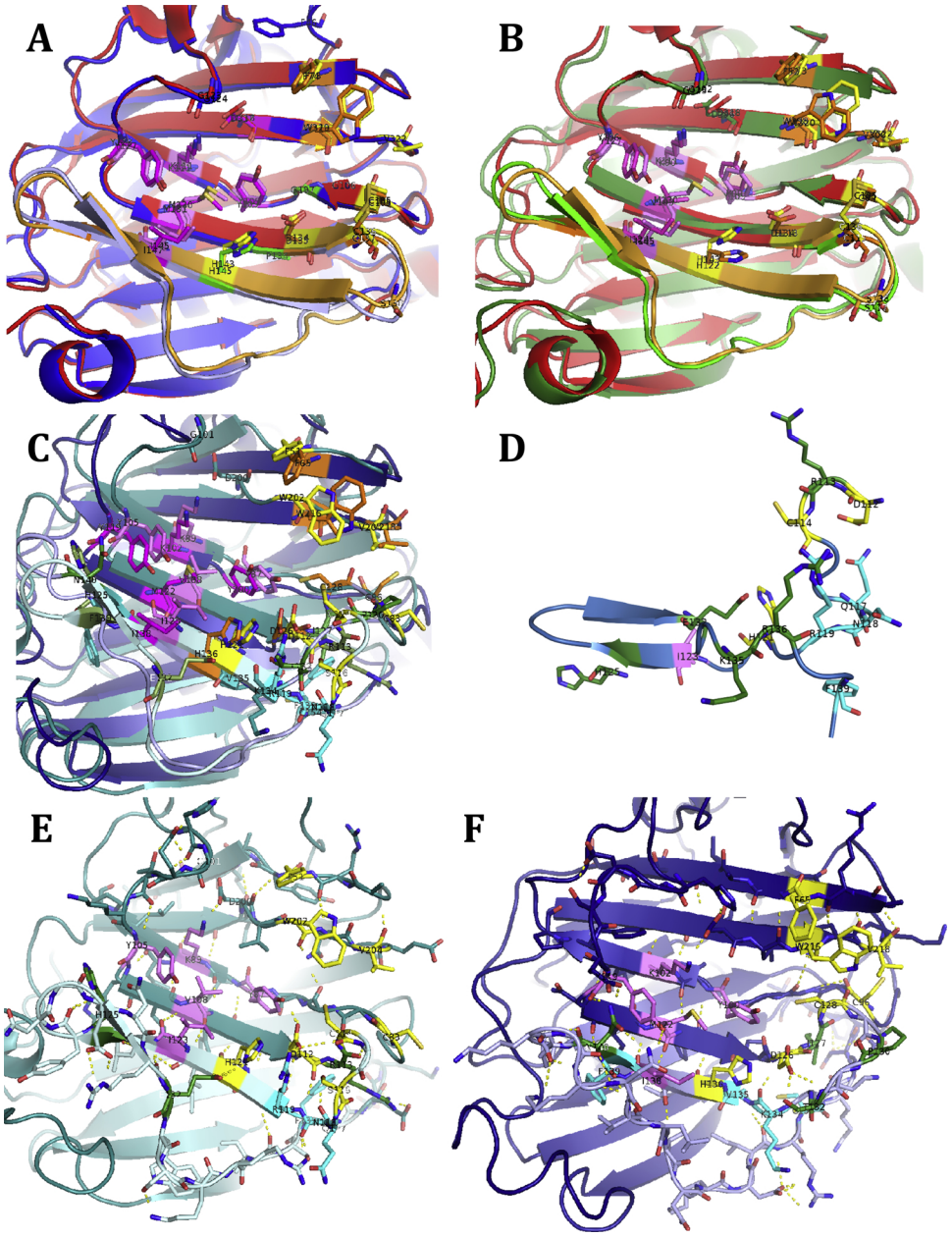

Fig. 6. Active sites mapping of TcCalr and HuCALR. A and B represent structures before molecular dynamics, and C to F after MD. GBS residues are colored pink or magenta, and PBS residues are yellow or orange, related to the first and second model in each case. Other residues involved in the sites are colored cyan and green. (A) Structural alignment of 5HCF (red) and 3POW (blue) PDB models. (B) Structural alignment of 5HCF (red) and TcCalr-SS-KEDL-ROBETTA_1*in silico* model (green). (C) Structural alignment of GCG-TcCalr-SS-C_KEDL_ROBETTA_SWISS_H_postMD (deep teal) and HuCALR-3POS_SWISS_H-postMD (deep blue) *in silico* models (Li et al., 2007). (D) Vc-TcCalr-SS-C_KEDL_RO-BETTA_SWISS_H_postMD (sky blue) *in silico* model. (E) Polar contacts in GCG-TcCalr-SS-C_KEDL_ROBETTA_SWISS_H_postMD. (F) Polar contacts in HuCALR-3POS_SWISS_H-postMD. Proteins and peptides were depicted with the PyMOL suite (www.pymol.org) (Chouquet et al., 2011). (For interpretation of the references to colour in the figure legend, the reader is referred to the web version of this article.)

mentioned do not form a pocket, a synergistic interaction is possible. Thus, when there is no glucose at the GBS, it can act in synergy with PBS in order to bind peptides. Reciprocally, PBS aids GBS to bind the substrate G1M3 (glucose-mannan$_3$) (Kozlov et al., 2010). These facts introduce a degree of complexity to determine the precise function of both subsites (Chouquet et al., 2011; Pocanschi et al., 2011; Wijeyesakere et al., 2013). As seen in Fig. 6A, the subsite mapping of 3POW and 5CHF are almost identical in residues and spatial conformation. Therefore, it is possible to map these subsites in TcCalr-SS-KEDL_ROBETTA_1, before and after MD, and compare them with the crystallographic models.

When the subsite mapping of 5CHF is followed in TcCalr-SS-KEDL_ROBETTA_1 (Fig. 6B), the most relevant residues have similar positions and orientations, with the exception of W320-W298 (*cis-trans* conformations) and H143-H122 (differing in approximately 40°). Thus, the TcCalr-SS-KEDL_ROBETTA_1 residues involved in the GBS site are Y88, K90, G102, Y106, V109, I124 and D296 and the ones involved in the PBS site are F52, C84, D113, C115, S117, H122, W298 and V300, with D113, C115, S117, H122 and I124 located at the start/end coils and at the central beta strand of the VC-TcCalr zone.

Moreover, the post-MD data, shown in Fig. 6C by the GCG-TcCalr-SS-C_KEDL_ROBETTA_SWISS_H_postMD *in silico* model, evidences other residues close to the GBS and PBS sites also playing a role in this dynamic (positions of the residues are shifted in -1 regarding TcCalr-SS-KEDL_ROBETTA_1 model). The TcCalr MD trajectory data (.dcd file) shows several residues constantly approaching at a distance smaller than 3.5 Å of GBS and PBS residues: E132 to H121 and I123, H125 to Y105 and I123 and R113 to C83, D112, C114, S116 and W202. In addition, the hydrogen bond network study (Fig. 4A) shows D112, C114, S116 and H121 at hydrogen-bonding distance from Q117, N118, R119, E132 and F139 start/end coils residues. Therefore, R113, Q117, N118, R119, H125, E132 and F139 can be considered as part of the TcCalr active site residues.

Regarding the isolated VC-TcCalr structure, Vc-TcCalr-SS-C_KEDL_ROBETTA_SWISS_H_postMD *in silico* model in Fig. 6D, D112 and H121, part of the PBS site, are also highly RMSD-correlated with other spatially close residues, K135 interacts predominantly with the central coils (beta strand in the whole model), and R136 interacts very

frequently with the start/end coils, which suggests a function as part of the TcCalr active site. Consequently, since several residues in the VC-TcCalr peptide share the same dynamics and interactions as in the whole protein, it is expected that the VC-TcCalr peptide conserves at least part of the antiangiogenic and antitumor properties displayed by the whole TcCalr.

HuCALR-3POS after MD (Fig. 6C) evidences that Hu_M122 (different from Tc_V108) and Hu_P130 (different from Tc_S116, not considered in this analysis) are not conserved at the TcCalr active site. Additionally, the residues that approach to GBS and PBS during the MD are I127, P130, T132 and N140. Furthermore, the hydrogen bond network (Fig. 4B) shows D126, C128, H136 and I138 close to I127, T132, K134, V135, F139 and C154 in the start/end coils. Lastly, N140 approaches the beta-turn. Therefore, I127, P130, T132, K134, V135, F139, N140 and C154 were added to the HuCALR active site as additional candidate residues.

All TcCalr and HuCALR relevant putative residues at their active sites were identified. Fig. 6C shows that their differences are not related to specific positions but to substitutions. Thus, amino acid substitutions generate a more rigid TcCalr, as compared to a more flexible HuCALR.

Identification of TcCalr and HuCALR active sites allows us to propose the presence of a binding site for collagenous tails like those present in the C1q stem. Indeed, partial cloning of C1 domains indicates that C1s establishes an important contact with C1q at specific sites (Girija et al., 2013). Although the degree of conservation of C1q is relatively low amongst higher vertebrates, the C-terminal half of its collagenous domain contains a hexapeptide motif present in all species: OGKXGP/Y/N (O is hydroxyproline and X is any amino acid), that mediates binding of C1r and C1s to six sites in the C1q heterotrimeric A-B-C chains (Bally et al., 2009; Phillips et al., 2009; Reid, 1979; Wallis et al., 2004). In human C1q, this motif is present in its three chains: once in C1qA (OGKVGY), once in C1qB (OGKVGP) and twice in C1qC (OGKDGY, OGKNGP) (Son et al., 2015; van Schaarenburg et al., 2016). In Fig. 1 from Girija et al. (2013), their three collagen-like peptides (a, b and c) form a D-helix with a characteristic one residue stagger between adjacent strands. Each chain has a very conserved K15 residue that binds C1s, in a characteristic binding pocket.

Mutagenesis data evidence that Kb61 y Kc58 are also essential for binding, while Ka59 is less important and may not bind to C1r or C1s (Bally et al., 2013). Vb62 or Nc59, together with the important lysine residues, could also enter into the C1s binding pocket in an intermediate adjustment state. By analogy, the four CUB1 domains (two for each C1r and C1s) would contact the two C1r CUB2 domains through other lysines when the C1r-C1s tetramer binds to C1q, thus explaining why Yb61 y Yc58 are essential for the formation of the C1 complex. Consequently, as lysine ends in a positive antenna-like structure and the binding pocket has several oxygen atoms binding to this antenna, it can be assumed that TcCalr and HuCALR binding location would have the same negative contacts with oxygen atoms from negative groups to allow the binding of C1q positive residues.

As a result, TcCalr and HuCALR possible binding pockets would be probably found in a site with several polar contacts and oxygen atoms between their GBS and PBS. The beta-turn is not considered in this analysis due to the hydrogen bonds that stabilize the turn, so they would not participate in binding other molecules. For TcCalr, the start/end coils site (part of its PBS) has more polar contacts and oxygen atoms, but the GBS has fewer and more distant contacts, rendering this zone inadequate to bind C1q. In HuCALR, Fig. 6F, although GBS has one more polar contact, the oxygen atoms are far away from each other and the PBS has a more flexible and open conformation than TcCalr, thus hindering possible contacts.

Therefore, it is likely that the PBS TcCalr site is more suited to bind to rigid and charged structures like collagenous tails (especially C1q) because both molecules share these same properties. This could be related with a higher TcCalr capacity to inhibit the pro-angiogenic mechanisms in endothelial cells and, as a consequence, a better antitumor effect. On the other hand, the more flexible HuCALR, and possibly calreticulin from all mammal species, can putatively bind to a larger variety of proteins, in agreement with its chaperone activity required by complex mammalian cells.

From these analyses, we determined the smallest TcCalr-derived peptide able to mediate the antiangiogenic properties of the whole parasite chaperone, with minimum potential immunogenicity, VC-TcCalr (DRCGSQNRVHIILHYNGENREWSKRISFP). Thus, VC-TcCalr and VC-HuCALR were chemically synthesized for *in vitro* and *in vivo* studies to be correlated with the results obtained *in silico*.

3.4. rTcCalr, VC-TcCalr and VC-HuCALR in vitro and in vivo assays

TcCalr binds to human C1q, inhibits the activation of the classical complement pathway in fluid phase (Ferreira et al., 2004b), binds to solid phase-bound human IgG, a natural activating ligand of C1 (Valck et al., 2010) and inhibits angiogenesis in the *Gallus gallus* chick embryonic chorioallantoic membrane (CAM) assay (Molina et al., 2005). In this capacity and equimolarly, TcCalr is more potent than HuCALR (Toledo et al., 2010). VC-TcCalr encompasses about half of the residues present in the active zone of both vasostatin and the 120-180 Cal fragment (VL-HuCALR) (Pike et al., 1999, 1998) that would bind to collagenous tails and exert the antiangiogenic and antitumor properties, and is similar to the active fragment of vasostatin (VC-HuCALR) (Li et al., 2007). For these reasons, it would be expected that by increasing the VC-TcCalr concentration, a strength similar to the whole TcCalr would be generated. Thus, to test this possibility, VC-TcCalr, VC-HuCALR, whole rTcCalr and scrambled VC-TcCalr (a negative control) were bound to a solid phase to capture C1q and then instilled to fertilized hen eggs in a CAM assay.

As seen in Fig. 7, left, 2 μg/ml of C1q bound to 1.28 μM of rTcCalr is not significantly different from 2.56 μM of VC-TcCalr or VC-HuCALR. However, with 1 μg/ml of C1q, TcCalr binds to C1q with 79% of the peptides binding strength without significant differences between them. These facts suggest that a double concentration of the peptides may compensate or outperform the binding strength to C1q displayed by the whole protein.

Furthermore, in Fig. 7, right, both 2.157×10^{-13} mol (10 ng/10 ml per filter) of rTcCalr and 4.313×10^{-13} mol (1.517 ng/10 ml per filter) of VC-TcCalr inhibited angiogenesis without significant differences, as compared to 4.313×10^{-13} mol (1.517 ng/10 ml) of scrambled VC-TcCalr (TS), a negative control. PBS-BSA, also a negative control, was added following the guidelines from Li et al. (2007) and Pike et al. (1999, 1998), using 1.11×10^{-11} moles of BSA diluted in PBS (738.5 ng/10 ml per filter) instead of ovalbumin. Its antiangiogenic effect can be explained by their high concentration compared to the other samples that probably saturated the filter. A higher statistical significance could not be achieved using this test due to the basal irreversible angiogenesis caused by sample instillation. Taken altogether, these data suggest that VC-TcCalr has a moderate antiangiogenic effect.

4. Discussion

Several anti-tumor HuCALR-derived fragments have been proposed (Li et al., 2007; Pike et al., 1999, 1998). Whole TcCalr also shares these properties. Trypanosomatids diverged about 231-283 million years ago, largely before hominids and most mammals (De Souza et al., 2018). The need to successfully cope with a variety of powerful immune attacks was urgent for the parasites and the TcCalr coding genes and probably other parasite genes, may have evolved accordingly. Mammal calreticulins, HuCALR included, were not necessarily subjected to these pressures. It is likely that these TcCalr capacities are coded and expressed in precise fragments at the DNA and the primary protein structure may be similar but probably different from the human ortholog molecules. Thus, the results presented here propose a structural explanation why TcCalr is equimolarly more potent than HuCALR in its

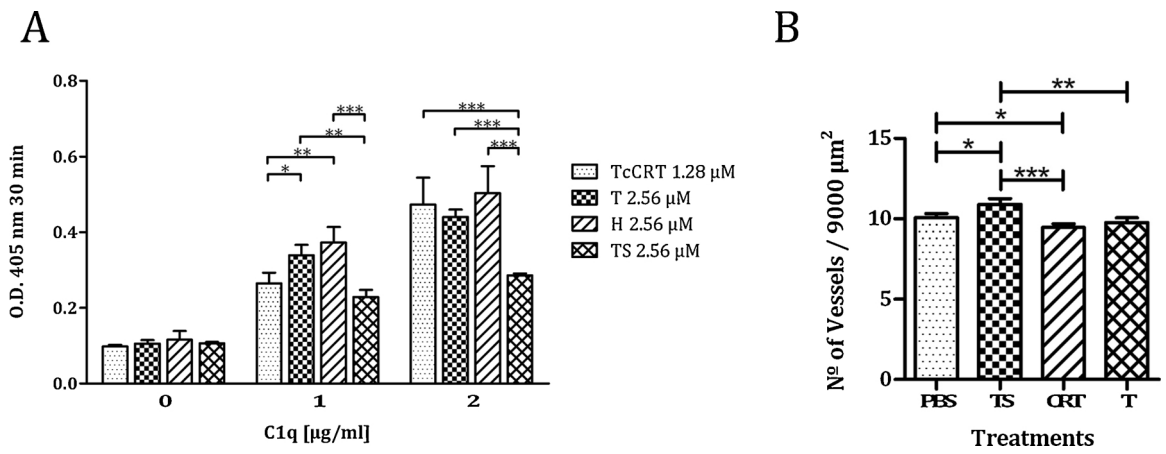

Fig. 7. TcCalr and VC-TcCalr binding and antiangiogenic properties. A) C1q binding to immobilized TcCalr and peptides. C1q was captured by solid phase-bound rTcCalr (TcCRT), VC-TcCalr (T), VC-HuCALR (H) and scrambled VC-TcCalr (TS). Increasing C1q concentrations were added and its binding to the peptides was detected with a goat anti-human C1q polyclonal antiserum. The results were analyzed by two-way ANOVA test and Bonferroni posttest. Each assay was performed in triplicates. A) rTcCalr and VC-TcCalr antiangiogenic results in the CAM assay. rTcCalr and PBS-BSA were added on filters as positive and negative controls, respectively. Also, VC-TcCalr (T) and scrambled VC-TcCalr (TS) were added on filters doubling rTcCalr concentration. The blood vessels present in 9000 μm^2 were counted in a double-blind procedure by conventional light microscopy. The results were analyzed by unpaired one-tailed t test. Bars represent the standard deviations of the means.

antiangiogenic and antitumor properties. *In silico* structural bioinformatic tools were used to also propose a TcCalr candidate peptide mediating, in equimolar terms, about half of the whole protein antiangiogenic and antitumor power.

Human, *T. cruzi,* murine and lapine calreticulins were aligned using BLASTP, COBALT, CLUSTALW2 and CLUSTAL OMEGA to study their similarity. By this means, the TcCalr location homologue to the vasostatin-like human peptide with antiangiogenic and antitumor function, VC-TcCalr, was found (Fig. 1) (Li et al., 2007; Pike et al., 1999, 1998).

Then, several *in silico* structural protein models were generated. The best one, TcCalr-SS-KEDL_ROBETTA_1, was obtained using the ROBETTA web server, shown in Fig. 2A. Its structural quality was checked in the SWISS-MODEL and WHAT IF web servers, verifying its native-protein-like properties and calreticulin-like conformation (Fig. 2B).

To approach its theoretical behavior in mammal blood and increase the structural quality of the regions within the calreticulins, molecular dynamics simulations (MD) were performed on VC-TcCalr, GCG-TcCalr (TcCalr globular domain without its P-domain and C-domain last residues) and HuCALR-3POS. The energetic environment of their amino acids was improved, its unfavorable energy was decreased, and the quality of the more compromised sectors was increased, yielding even better models (Fig. 3) and explaining the parasite and human calreticulins variabilities. Also, concerted movement at their short vasostatin-like sites and vicinities, hydrogen bond networks (Fig. 4) and electrostatic potential and fields (Fig. 5), were studied. On the one hand, as shown in Fig. 5A, the residues directed towards TcCalr interior are non-polar, while the concave face, directed towards the external media, is very polar, its beta-turn (located at the center of VC-Calr primary sequence) is stabilized by several saline bridges and has at the opposite end an electrostatic field favoring interactions with the start/end coils (VC-Calr first and last residues coils). All these properties provide this zone with a rigid dipolar nature, more favorable to interact with other rigid polar proteins such as collagenous tails. On the other hand, Fig. 5Bb shows that VC-HuCALR possesses zones with weaker and opposite superficial charges and polarity, as compared to TcCalr, and an electrostatic field favoring the interactions towards the beta-turn, also opposite to TcCalr. This is mainly explained by the substitutions of at least Q117 by G131, R119 by K134, R136 by D151 and S138 by R153 that relax the structure, turning it more flexible and thus less favorable to interact with other rigid domains but more adequate to bind to a broader range of proteins.

This evidence concurs with recent literature that localizes the TcCalr and HuCALR lectin-type binding active sites: the glucose-binding site (GBS), located at the center of its concave face, and the peptide binding site (PBS) (Moreau et al., 2016), located at the opposite edge, at the start/end coils (Fig. 6A). When mapping both sites on the models (TcCalr-SS-KEDL_ROBETTA_1 is very similar to TcCalr-5HCF, completing its final primary sequence, Fig. 6B and C), Fig. 6E shows that TcCalr PBS and start/end coils have negative side chains with close oxygen atoms mediating hydrogen bonds that yield a rigid structure and a stable center, able to bind positive residues such as the lysine present in the C1q collagenous stalk that interacts with C1s (Girija et al., 2013). HuCALR should be less efficient to accomplish this function, most likely because both active sites relax, separating PBS oxygen atoms and preventing a better interaction with the C1q-collagenous tail (Fig. 6F).

Thus TcCalr, rigid and dipolar, would have a more favorable and stable binding to other proteins with similar nature, such as collagenous tails, required for the inhibition of angiogenesis. HuCALR, more flexible and less polar, would have a less favorable binding to collagenous tails but more favorable to a wider range of proteins, required by its complex chaperone and protein quality control activities in the mammal cell ER. In other words, TcCalr has bigger antiangiogenic and antitumor activities than HuCALR because of its amino acidic substitutions that modify its ionic, polar, hydrophobic and hydrogen bond interactions, stabilizing its active sites in a better way, specially its PBS.

TcCalr has a potential to induce tumor immunogenicity, due to its extensive differences with HuCALR in their primary amino acidic sequence. These differences are also valid with calreticulins from many other vertebrates (in fact, TcCalr is more similar and phylogenetically closer to *Arabidopsis thaliana* Calr than to mammal Calr (Weinberger et al., 2017)). Moreover, TcCalr has an inherent property to bind to all tumor cells we have studied so far (murine, human and canine mammary adenocarcinomas, murine melanoma and canine transmissible venereal tumor (Cruz et al., 2019,unpublished; Sosoniuk-Roche et al., 2019,unpublished). TcCalr recruits C1q at the tumor surface, generating “eat-me” signals for phagocytes and dendritic cells. We propose that these may be essential first steps to mount an anamnestic adaptive anti-tumor immune response, with cytotoxic and/or helper T cells cohorts mobilization, specific to TcCalr derived peptides and/or tumor-specific antigens not yet identified (Ramírez-Toloza et al., 2016). In agreement with the previous sections, the VC-TcCalr and VC-HuCALR peptides were used in the solid phase-bound protein-peptide *in vitro* and

in the CAM *in ovum* assays. In the former (Fig. 7A), there was no difference between the binding of 1.28 μM rTcCalr and twice the moles of the peptides to 2 μg/ml of C1q, but 1.28 μM of rTcCalr binds to 1 μg/ml of C1q with 79% the strength of 2.56 μM of the peptides. In the latter (Fig. 7B), the VC-TcCalr antiangiogenic action was confirmed. Both results, taken together, suggest that twice the molarity of VC-TcCalr can equate and even outperform the power of whole TcCalr in the binding to C1q and the execution of their antiangiogenic effect.

Therefore, the antiangiogenic and antitumor activity of *T. cruzi* calreticulin seems to be delimited by a precise subdomain in its N-terminal domain and localized at its concave face: VC-TcCalr, encompassing amino acids 131-159, more stable than VC-HuCALR, in its interaction with rigid and charged domains like collagenous tails.Perhaps, better TcCalr antiangiogenic and antitumor activities, allows *T. cruzi* to protect its hosts from the lethal actions of highly prevalent solid malign tumors. A protected host allows the parasite to reproduce an expand its genome.

TcCalr potential usefulness as antitumor prophylactic and potentially therapeutic agent, requires additional experimental studies at a preclinical level. Comparisons of the effects of the whole recombinant human and parasite proteins are necessary, as well as that of the 29-amino acid VC-TcCalr peptide. The main advantages of using the peptide instead of the whole protein reside in its more robust production and easier validation and application processes, together with a lower immunogenicity. On the other hand, the peptide capacity to force tumor immunogenicity, would be necessarily lower than that of the whole parasite molecule. These capacities should be compared in vivo, at equimolar terms.

Perspectives of this work may focus on: i) TcCalr structural studies by the *in silico* docking with C1, scavenger receptors or other molecules; ii) testing VC-TcCalr antiangiogenic and antitumor activities further to assess an antitumor function besides its antiangiogenic activity by its subcutaneous and intravenous administration in A/J mice bearing TA3 MTXR mammary adenocarcinoma cells, and iii) optimizing VC-TcCalr production by induced expression and VC-TcCalr random and site-specific mutagenesis to increase its activity.

There are several aspects of this *T. cruzi*-vertebrate interaction not elucidated yet, such as TcCalr S domain physicochemical properties, located at the TcCalr convex face, opposite to the active sites studied here, that has anticomplement activity, and its flexible P domain, with lectin and calcium storage activities.

Finally, it is necessary to continue these studies to better understand how *T. cruzi* protects its hosts against several solid tumor types, mammary in particular, by TcCalr and other proteins. The unique capacity of *T. cruzi* to translocate its chaperone to the exterior unleashes all these surprising features.

Declaration of competing interests

The authors declare no financial or commercial conflict of interest.

Acknowledgments

This work was supported by Chilean Public Grants 1130099 (A. Ferreira), 1141311 (A. Olivera-Nappa) from FONDECYT-CHILE, CONICYT PIA Basal Funding for Excellence Scientific and Technological Centers CeBiB FB0001 (J. Asenjo, A. Olivera-Nappa) and VID-Universidad de Chile (A. Ferreira). J. Peña received a CONICYT Fellowship for Doctoral Training.

References

Abello-Cáceres, P., Pizarro-Bauerle, J., Rosas, C., Maldonado, I., Aguilar-Guzmán, L., González, C., Ramírez, G., Ferreira, J., Ferreira, A., 2016. Does native *Trypanosoma cruzi* calreticulin mediate growth inhibition of a mammary tumor during infection? BMC Cancer 16, 731. https://doi.org/10.1186/s12885-016-2764-5.

Aguillón, J.C., Ferreira, L., Pérez, C., Colombo, A., Molina, M.C., Wallace, A., Solari, A., Carvallo, P., Galindo, M., Galanti, N., Örn, A., Billetta, R., Ferreira, A., 2000. Tc45, a dimorphic *Trypanosoma cruzi* immunogen with variable chromosomal localization, is calreticulin. Am. J. Trop. Med. Hyg. 63, 306–312.

Anandakrishnan, R., Aguilar, B., Onufriev, A.V., 2012. H++ 3.0: automating pK prediction and the preparation of biomolecular structures for atomistic molecular modeling and simulations. Nucleic Acids Res. 40 (W1), W537–W541.

Atayde, V.D., Jasiulionis, M.G., Cortez, M., Yoshida, N., 2008. A recombinant protein based on *Trypanosoma cruzi* surface molecule gp82 induces apoptotic cell death in melanoma cells. Melanoma Res. 18 (3), 172–183. https://doi.org/10.1097/CMR.0b013e3282feeaab.

Baird, J.R., Byrne, K.T., Lizotte, P.H., Toraya-Brown, S., Scarlett, U.K., Alexander, M.P., Sheen, M.R., Fox, B.A., Bzik, D.J., Bosenberg, M., Mullins, D.W., Turk, M.J., Fiering, S., 2013. Immune-Mediated Regression of Established B16F10 Melanoma by Intratumoral Injection of Attenuated Toxoplasma gondii Protects against Rechallenge. J. Immunol. 190 (1), 469–478. https://doi.org/10.4049/jimmunol.1201209.

Baker, N.A., Sept, D., Joseph, S., Holst, M.J., McCammon, J.A., 2001. Electrostatics of nanosystems: application to microtubules and the ribosome. Proc. Natl. Acad. Sci. U. S. A. 98, 10037–10041. https://doi.org/10.1073/pnas.181342398.

Bally, I., Ancelet, S., Moriscot, C., Gonnet, F., Mantovani, A., Daniel, R., Schoehn, G., Arlaud, G.J., Thielens, N.M., 2013. Expression of recombinant human complement C1q allows identification of the C1r/C1s-binding sites. Proc. Natl. Acad. Sci. U. S. A. 110, 8650–8655. https://doi.org/10.1073/pnas.1304894110.

Bally, I., Rossi, V., Lunardi, T., Thielens, N.M., Gaboriaud, C., Arlaud, G.J., 2009. Identification of the C1q-binding sites of human C1r and C1s. A refined three-dimensional model of the C1 complex of complement. J. Biol. Chem. 284, 19340–19348. https://doi.org/10.1074/jbc.M109.004473.

Benkert, P., Biasini, M., Schwede, T., 2011. Toward the estimation of the absolute quality of individual protein structure models. Bioinformatics 27, 343–350. https://doi.org/10.1093/bioinformatics/btq662.

Benkert, P., Künzli, M., Schwede, T., 2009a. QMEAN server for protein model quality estimation. Nucleic Acids Res. 37, 1–5. https://doi.org/10.1093/nar/gkp322.

Benkert, P., Tosatto, S.C.E., Schwede, T., 2009b. Global and local model quality estimation at CASP8 using the scoring functions QMEAN and QMEANclust. Proteins Struct. Funct. Bioinforma. 77, 173–180. https://doi.org/10.1002/prot.22532.

Biasini, M., Bienert, S., Waterhouse, A., Arnold, K., Studer, G., Schmidt, T., Kiefer, F., Cassarino, T.G., Bertoni, M., Bordoli, L., Schwede, T., 2014. SWISS-MODEL: Modelling protein tertiary and quaternary structure using evolutionary information. Nucleic Acids Res. 42, 252–258. https://doi.org/10.1093/nar/gku340.

Cabral, H.R.A., 2000. The tumoricidal effect of *Trypanosoma cruzi*: its intracellular cycle and the immune response of the host. Med. Hypotheses 54 (1), 1–6. https://doi.org/10.1054/mehy.1998.0808.

Camidge, R., Krementsov, N., 2002. The cure. a story of cancer and politics from the annals of the cold war. BMJ. Chicago 324 (7353), 1589. https://doi.org/10.1136/bmj.324.7353.1589/a.

Chen, Lili, He, Z., Qin, L., Li, Q., Shi, X., Zhao, S., Chen, Ling, Zhong, N., Chen, X., 2011. Antitumor effect of malaria parasite infection in a murine lewis lung cancer model through induction of innate and adaptive immunity. PLoS One 6 (9), e24407. https://doi.org/10.1371/journal.pone.0024407.

Chouquet, A., Païdassi, H., Ling, W.L., Frachet, P., Houen, G., Arlaud, G.J., Gaboriaud, C., 2011. X-ray structure of the human calreticulin globular domain reveals a peptide-binding area and suggests a multi-molecular mechanism. PLoS One 6, 1–9. https://doi.org/10.1371/journal.pone.0017886.

Coura, J.R., 2006. [Transmission of chagasic infection by oral route in the natural history of Chagas disease]. Rev Soc Bras Med Trop 39 Suppl 3, 113–117.

Coura, J.R., Viñas, P.A., 2010. Chagas disease: a new worldwide challenge. Nature 465, S6–S7. https://doi.org/10.1038/nature09221.

Cruz P., Sosoniuk-Roche E., Maldonado I., Torres C., Ferreira A., Trypanosoma cruzi calreticulin: in vitro modulation of key immunogenic markers of both canine tumors and relevant competent cells, unpublished, 2019.

DeLano, W.L., 2002. The PyMOL Molecular Graphics System. Schrödinger LLC Version 1. http://www.pymol.org.

De Souza, D.A.S., Pavoni, D.P., Krieger, M.A., Ludwig, A., 2018. Evolutionary analyses of myosin genes in trypanosomatids show a history of expansion, secondary losses and neofunctionalization. Sci. Rep. 8 (1), 1376. https://doi.org/10.1038/s41598-017-18865-y.

Dolinsky, T.J., Czodrowski, P., Li, H., Nielsen, J.E., Jensen, J.H., Klebe, G., Baker, N.A., 2007. PDB2PQR: expanding and upgrading automated preparation of biomolecular structures for molecular simulations. Nucleic Acids Res. 35, 522–525. https://doi.org/10.1093/nar/gkm276.

Dolinsky, T.J., Nielsen, J.E., McCammon, J.A., Baker, N.A., 2004. PDB2PQR: An automated pipeline for the setup of Poisson-Boltzmann electrostatics calculations. Nucleic Acids Res. 32, 665–667. https://doi.org/10.1093/nar/gkh381.

Ferreira, V., Molina, M.C., Schwaeble, W., Lemus, D., Ferreira, A., 2005. Does Trypanosoma cruzi calreticulin modulate the complement system and angiogenesis? Trends Parasitol. 21, 169–174. https://doi.org/10.1016/j.pt.2005.02.005.

Ferreira, V., Molina, M.C., Valck, C., Rojas, Á., Aguilar, L., Ramírez, G., Schwaeble, W., Ferreira, A., 2004a. Role of calreticulin from parasites in its interaction with vertebrate hosts. Mol. Immunol. 40, 1279–1291. https://doi.org/10.1016/j.molimm.2003.11.018.

Ferreira, V., Molina, M.C., Valck, C., Rojas, Á., Ferreira, A., 2002. Parasite calreticulin: possible roles in the parasite/host interface. Inmunología 21, 156–168.

Ferreira, V., Valck, C., Sánchez, G., Gingras, A., Tzima, S., Molina, M.C., Sim, R., Schwaeble, W., Ferreira, A., 2004b. The classical activation pathway of the human complement system is specifically inhibited by calreticulin from *Trypanosoma cruzi*. J.

Immunol. 172, 3042–3050. https://doi.org/10.4049/jimmunol.172.5.3042.
Flores-Chávez, M., Fernández, B., Puente, S., Torres, P., Rodríguez, M., Monedero, C., Cruz, I., Gárate, T., Cañavate, C., 2008. Transfusional chagas disease: parasitological and serological monitoring of an infected recipient and blood donor. Clin. Infect. Dis. 46, e44–7. https://doi.org/10.1086/527448.
Folkman, J., 2003. Fundamental concepts of the angiogenic process. Curr. Mol. Med. 3, 643–651. https://doi.org/10.2174/1566524033479465.
Freilij, H., Altcheh, J., 1995. Congenital Chagas' disease: diagnostic and clinical aspects. Clin Infect Dis 21, 551–555.
Girija, U.V., Gingras, A.R., Marshall, J.E., Panchal, R., Sheikh, M.A., Gál, P., Schwaeble, W.J., Mitchell, D. a., Moody, P.C.E., Wallis, R., 2013. Structural basis of the C1q/C1s interaction and its central role in assembly of the C1 complex of complement activation. Proc. Natl. Acad. Sci. 110 (34), 13916–13920. https://doi.org/10.1073/pnas.1311113110.
Gordon, J.C., Myers, J.B., Folta, T., Shoja, V., Heath, L.S., Onufriev, A., 2005. H++: A server for estimating pKas and adding missing hydrogens to macromolecules. Nucleic Acids Res. 33, W368–W371. https://doi.org/10.1093/nar/gki464.
Hauschka, T.S., Goodwin, M.B., 1948. *Trypanosoma cruzi* endotoxin (KR) in the treatment of malignant mouse tumors. Science 107, 600–602. https://doi.org/10.1126/science.107.2788.600.
Holst, M., Saied, F., 1993. Multigrid solution of the Poisson-Boltzmann equation. J. Comput. Chem. 14, 105–113. https://doi.org/10.1002/jcc.540140114.
Humphrey, W., Dalke, A., Schulten, K., 1996. VMD: visual molecular dynamics. J. Mol. Graph. Model. 14https://doi.org/10.1016/0263-7855(96)00018-5. 27–28, 33–38.
Hunter, C.A., Yu, D., Gee, M., Ngo, C.V., Sevignani, C., Goldschmidt, M., Golovkina, T.V., Evans, S., Lee, W.F., Thomas-Tikhonenko, A., 2001. Cutting edge: systemic inhibition of angiogenesis underlies resistance to tumors during acute toxoplasmosis. J. Immunol. 166 (10), 5878–5881. https://doi.org/10.4049/jimmunol.166.10.5878.
Junqueira, C., Guerrero, A.T., Galvão-Filho, B., Andrade, W.A., Salgado, A.P.C., Cunha, T.M., Ropert, C., Campos, M.A., Penido, M.L.O., Mendonça-Previato, L., Previato, J.O., Ritter, G., Cunha, F.Q., Gazzinelli, R.T., 2012. *Trypanosoma cruzi* adjuvants potentiate T cell-mediated immunity induced by a NY-ESO-1 based antitumor vaccine. PLoS One 7 (5), e36245. https://doi.org/10.1371/journal.pone.0036245.
Junqueira, C., Santos, L.I., Galvão-Filho, B., Teixeira, S.M., Rodrigues, F.G., DaRocha, W.D., Chiari, E., Jungbluth, A.A., Ritter, G., Gnjatic, S., Old, L.J., Gazzinelli, R.T., 2011. Trypanosoma cruzi as an effective cancer antigen delivery vector. Proc. Natl. Acad. Sci. U. S. A. 108, 19695–19700. https://doi.org/10.1073/pnas.1110030108.
Kalé, L., Skeel, R., Bhandarkar, M., Brunner, R., Gursoy, A., Krawetz, N., Phillips, J., Shinozaki, A., Varadarajan, K., Schulten, K., 1999. NAMD2: greater scalability for parallel molecular dynamics. J. Comput. Phys. 151, 283–312. https://doi.org/10.1006/jcph.1999.6201.
Kallinikova, V.D., Matekin, P.V., Ogloblina, T.A., Leikina, M.I., Kononenko, A.F., Sokolova, N.M., Pogodina, L.S., 2001. Anticancer properties of flagellate protozoan *Trypanosoma cruzi* Chagas, 1909. Biol. Bull. 28, 244–255. https://doi.org/10.1023/A:1016636419597.
Kim, D.E., Chivian, D., Baker, D., 2004. Protein structure prediction and analysis using the Robetta server. Nucleic Acids Res. 32, 526–531. https://doi.org/10.1093/nar/gkh468.
Klyuyeva, N.G., Roskin, G.I., 1963. Biotherapy of malignant tumours. The MacMillan Co.
Kozlov, G., Pocanschi, C.L., Rosenauer, A., Bastos-Aristizabal, S., Gorelik, A., Williams, D.B., Gehring, K., 2010. Structural basis of carbohydrate recognition by calreticulin. J. Biol. Chem. 285, 38612–38620. https://doi.org/10.1074/jbc.M110.168294.
Krementsov, N., 2009. *Trypanosoma cruzi*, cancer and the Cold War. Hist. Cienc. Saude. Manguinhos. 16 Suppl 1, 75–94. https://doi.org/10.1590/S0104-59702009000500005.
Kun, H., Moore, A., Mascola, L., Steurer, F., Lawrence, G., Kubak, B., Radhakrishna, S., Leiby, D., Herron, R., Mone, T., Hunter, R., Kuehnert, M., 2009. Transmission of *Trypanosoma cruzi* by heart transplantation. Clin. Infect. Dis. 48, 1534–1540. https://doi.org/10.1086/598931.
Lamerdin, J.E., McCready, P., Stilwagen, S., Ramirez, M., Carrano, A., 1996. Characterization by Genomic Sequence Analysis of a Gene-Rich 111 kb Region of 19p13.2 Containing the Human DNA Repair Gene, RAD23A. Unpublished.
Lemus, D., Dabancens, A., Illanes, J., Fuenzalida, M., Guerrero, A., López, C., 2001. Antiangiogenic effect of betamethasone on the chick cam stimulated by TA3 tumor supernatant. Biol. Res. 34, 227–236. https://doi.org/10.1088/1748-6041/4/4/044103.
Li, X., Jiang, L., Wang, Y., Xiao, Y., Huang, Y., Yao, Q., Yang, Y., Wu, X., 2007. Inhibition of angiogenesis by a novel small peptide consisting of the active fragments of platelet factor-4 and vasostatin. Cancer Lett. 256, 29–32.
López, N.C., Valck, C., Ramírez, G., Rodríguez, M., Ribeiro, C., Orellana, J., Maldonado, I., Albini, A., Anacona, D., Lemus, D., Aguilar, L., Schwaeble, W., Ferreira, A., 2010. Antiangiogenic and antitumor effects of *Trypanosoma cruzi* calreticulin. PLoS Negl. Trop. Dis. 4, 1–9. https://doi.org/10.1371/journal.pntd.0000730.
Malisoff, W.M., 1947. The action of the endotoxin of trypanosoma cruzi (KR) on malignant mouse tumors. Science 106 (2763), 591–594. https://doi.org/10.1126/science.106.2763.591-a.
Mel'nikov, V.G., Fierro Velasko, F.H., Dobrovinskaya, O.R., 2004. Suppression of growth and metastasizing of T-Cell lymphoma in mice infected with American trypanosomiasis at different stages of experimental infection. Bull. Exp. Biol. Med. 137 (5), 475–478. https://doi.org/10.1023/B:BEBM.0000038157.69208.27.
Melo, F., Feytmans, E., 2008. Scoring functions for protein structure prediction. Computational Structural Biology: Methods and Applications. pp. 61–68.
Michalak, M., Groenendyk, J., Szabo, E., Gold, L.I., Opas, M., 2009. Calreticulin, a multi-process calcium-buffering chaperone of the endoplasmic reticulum. Biochem. J. 417, 651–666. [pii]\r10.1042/BJ20081847. https://www.doi.org/BJ20081847.
Molina, M.C., Ferreira, V., Valck, C., Aguilar, L., Orellana, J., Rojas, A., Ramirez, G., Billetta, R., Schwaeble, W., Lemus, D., Ferreira, A., 2005. An in vivo role for Trypanosoma cruzi calreticulin in antiangiogenesis. Mol. Biochem. Parasitol. 140, 133–140. https://doi.org/10.1016/j.molbiopara.2004.12.014.
Moreau, C., Cioci, G., Iannello, M., Laffly, E., Chouquet, A., Ferreira, A., Thielens, N.M., Gaboriaud, C., 2016. Structures of parasite calreticulins provide insights into their flexibility and dual carbohydrate/peptide-binding properties. IUCrJ 3, 408–419. https://doi.org/10.1107/S2052252516012847.
Noya, V., Bay, S., Festari, M.F., García, E.P., Rodriguez, E., Chiale, C., Ganneau, C., Baleux, F., Astrada, S., Bollati-Fogolín, M., Osinaga, E., Freire, T., 2013. Mucin-like peptides from *Echinococcus granulosus* induce antitumor activity. Int. J. Oncol. 43 (3), 775–784. https://doi.org/10.3892/ijo.2013.2000.
Oikonomopoulou, K., Brinc, D., Hadjisavvas, A., Christofi, G., Kyriacou, K., Diamandis, E.P., 2014. The bifacial role of helminths in cancer: involvement of immune and non-immune mechanisms. Crit. Rev. Clin. Lab. Sci. 51, 138–148. https://doi.org/10.3109/10408363.2014.886180.
Oliveira, E.C., Leite, M.S., Miranda, J.A., Andrade, a L., Garcia, S.B., Luquetti, a O., Moreira, H., 2001. Chronic *Trypanosoma cruzi* infection associated with low incidence of 1,2-dimethylhydrazine-induced colon cancer in rats. Carcinogenesis 22, 737–740. https://doi.org/10.1093/carcin/22.5.737.
Pérez-Molina, J.A., Perez, A.M., Norman, F.F., Monge-Maillo, B., López-Vélez, R., 2015. Old and new challenges in Chagas disease. Lancet Infect. Dis. 15 (11), 1347–1356. https://doi.org/10.1016/S1473-3099(15)00243-1.
Phillips, A.E., Toth, J., Dodds, A.W., Girija, U.V., Furze, C.M., Pala, E., Sim, R.B., Reid, K.B.M., Schwaeble, W.J., Schmid, R., Keeble, A.H., Wallis, R., 2009. Analogous interactions in initiating complexes of the classical and lectin pathways of complement. J. Immunol. 182 (12), 7708–7717. https://doi.org/10.4049/jimmunol.0900666.
Phillips, J.C., Braun, R., Wang, W., Gumbart, J., Tajkhorshid, E., Villa, E., Chipot, C., Skeel, R.D., Kalè, L., Schulten, K., 2005. Scalable molecular dynamics with NAMD. J. Comput. Chem. 26, 1781–1802. https://doi.org/10.1002/jcc.20289.
Pike, S.E., Yao, L., Jones, K.D., Cherney, B., Appella, E., Sakaguchi, K., Nakhasi, H., Teruya-Feldstein, J., Wirth, P., Gupta, G., Tosato, G., 1998. Vasostatin, a calreticulin fragment, inhibits angiogenesis and suppresses tumor growth. J. Exp. Med. 188, 2349–2356. https://doi.org/10.1084/jem.188.12.2349.
Pike, S.E., Yao, L., Setsuda, J., Jones, K.D., Cherney, B., Appella, E., Sakaguchi, K., Nakhasi, H., Atreya, C.D., Teruya-Feldstein, J., Wirth, P., Gupta, G., Tosato, G., 1999. Calreticulin and calreticulin fragments are endothelial cell inhibitors that suppress tumor growth. Blood 94, 2461–2468.
Pocanschi, C.L., Kozlov, G., Brockmeier, U., Brockmeier, A., Williams, D.B., Gehring, K., 2011. Structural and functional relationships between the lectin and arm domains of calreticulin. J. Biol. Chem. 286, 27266–27277. https://doi.org/10.1074/jbc.M111.258467.
Plumelle, Y., Gonin, C., Edouard, A., Bucher, B.J., Thomas, L., Brebion, A., Panelatti, G., 1997. Effect of *Strongyloides stercoralis* infection and eosinophilia on age at onset and prognosis of adult T-cell leukemia. Am. J. Clin. Pathol. 107 (1), 81–87. https://doi.org/10.1093/ajcp/107.1.81.
Ramachandran, G.N., Ramakrishnan, C., Sasisekharan, V., 1963. Stereochemistry of polypeptide chain configurations. J. Mol. Biol. 7, 95–99. https://doi.org/10.1016/S0022-2836(63)80023-6.
Ramírez-Toloza, G., Abello, P., Ferreira, A., 2016. Is the antitumor property of *Trypanosoma cruzi* infection mediated by its calreticulin? Front. Immunol. 7, 1–8. https://doi.org/10.3389/fimmu.2016.00268.
Ramírez-Toloza, G., Aguilar-Guzmán, L., Valck, C., Abello, P., Ferreira, A., 2014. Is it all that bad when living with an intracellular protozoan? the role of *Trypanosoma cruzi* calreticulin in angiogenesis and tumor growth. Front. Oncol. 4, 382. https://doi.org/10.3389/fonc.2014.00382.
Ramírez, G., Valck, C., Ferreira, V.P., López, N., Ferreira, A., 2011. Extracellular *Trypanosoma cruzi* calreticulin in the host-parasite interplay. Trends Parasitol. 27, 115–122. https://doi.org/10.1016/j.pt.2010.12.007.
Ramos, R., Juri, M., Ramos, A., Hoecker, G., Lavandero, S., Pena, P., Morello, A., Repetto, Y., Aguillon, J.A., Ferreira, A., 1991. An immunogenetically defined and immunodominant *Trypanosoma cruzi* antigen. Am. J. Trop. Med. Hygiene 44 (3), 314–322.
Reid, B.K.B.M., 1979. Complete amino acid sequences of the three collagen-like regions present in subcomponent Clq of the first component of human complement. Biochem. J. 179, 367–371.
Reva, B.A., Finkelstein, A.V., Skolnick, J., 1998. What is the probability of a chance prediction of a protein structure with an rmsd of 6 Å? Fold. Des. 3, 141–147. https://doi.org/10.1016/S1359-0278(98)00019-4.
Rimoldi, M.T., Tenner, A.J., Bobak, D.A., Joiner, K.A., 1989. Complement component C1q enhances invasion of human mononuclear phagocytes and fibroblasts by *Trypanosoma cruzi* trypomastigotes. J. Clin. Invest. 84, 1982–1989. https://doi.org/10.1172/JCI114388.
Roskin, G., Exempliarskaia, E., 1931. Protozoeninfektion und experimenteller Krebs — I. Mitt. Z. Krebsforsch. 34, 628–645. https://doi.org/10.1007/BF01625403.
Roskin, G.I., 1946. Toxin therapy of experimental cancer: the influence of protozoan infections upon transplanted cancer. Cancer Res. 6, 363–365.
Schrag, J.D., Bergeron, J.J.M., Li, Y., Borisova, S., Hahn, M., Thomas, D.Y., Cygler, M., 2001. The structure of calnexin, an ER chaperone involved in quality control of protein folding. Mol. Cell 8, 633–644. https://doi.org/10.1016/S1097-2765(01)00318-5.
Sheklakova, L.A., Kallinikova, V.D., Karpenko, L.P., 2003. Genetic heterogeneity of Trypanosoma cruzi and its direct anticancer effect in cultured human tumor cells. Bull. Exp. Biol. Med. 135 (1), 89–92. https://doi.org/10.1023/A:1023466517225.
Sievers, F., Wilm, A., Dineen, D., Gibson, T.J., Karplus, K., Li, W., Lopez, R., McWilliam, H., Remmert, M., Söding, J., Thompson, J.D., Higgins, D.G., 2011. Fast, scalable generation of high quality protein multiple sequence alignments using Clustal

Omega. Mol. Syst. Biol. 7 (1).
Son, M., Diamond, B., Santiago-Schwarz, F., 2015. Fundamental role of C1q in autoimmunity and inflammation. Immunol. Res. 63, 101–106. https://doi.org/10.1007/s12026-015-8705-6.
Sosoniuk, E., Vallejos, G., Kenawy, H., Gaboriaud, C., Thielens, N., Fujita, T., Schwaeble, W., Ferreira, A., Valck, C., 2014. Trypanosoma cruzi calreticulin inhibits the complement lectin pathway activation by direct interaction with L-Ficolin. Mol. Immunol. 60, 80–85. https://doi.org/10.1016/j.molimm.2014.03.014.
Sosoniuk-Roche E., Cruz P., Maldonado I., Duaso L., Pesce B., Michalak M., Valck C., Ferreira A., In vitro treatment of a murine mammary adenocarcinoma cell line with recombinant Trypanosoma cruzi calreticulin promotes immunogenicity and phagocytosis, unpublished, 2019.
Stuart, G.R., Lynch, N.J., Day, A.J., Schwaeble, W.J., Sim, R.B., 1997. The C1q and collectin binding site within C1q receptor (cell surface calreticulin). Immunopharmacology 38, 73–80. https://doi.org/10.1016/S0162-3109(97)00076-3.
Stuart, G.R., Lynch, N.J., Lu, J., Geick, A., Moffatt, B.E., Sim, R.B., Schwaeble, W.J., 1996. Localisation of the C1q binding site within C1q receptor/calreticulin. FEBS Lett. 397, 245–249. https://doi.org/10.1016/S0014-5793(96)01156-8.
Tanowitz, H.B., Weiss, L.M., Montgomery, S.P., 2011. Chagas disease has now gone global. PLoS Negl. Trop. Dis. 5 (4), e1136. https://doi.org/10.1371/journal.pntd.0001136.
Toledo, V., Ramírez, G., Valck, C., López, N., Ribeiro, C.H., Maldonado, I., Aguilar, L., Lemus, D., Ferreira, A., 2010. Comparative in vivo antiangiogenic effects of calreticulin from *Trypanosoma cruzi* and *Homo sapiens*. Biol. Res. 43, 287–289. https://doi.org/10.4067/S0716-97602010000300004.
Ubillos, L., Freire, T., Berriel, E., Chiribao, M.L., Chiale, C., Festari, M.F., Medeiros, A., Mazal, D., Rondán, M., Bollati-Fogolín, M., Rabinovich, G.A., Robello, C., Osinaga, E., 2016. Trypanosoma cruzi extracts elicit protective immune response against chemically induced colon and mammary cancers. Int. J. Cancer. 138 (7), 1719–1731. https://doi.org/10.1002/ijc.29910.
Valck, C., Ramírez, G., López, N., Ribeiro, C.H., Maldonado, I., Sánchez, G., Ferreira, V.P., Schwaeble, W.J., Ferreira, A., 2010. Molecular mechanisms involved in the inactivation of the first component of human complement by Trypanosoma cruzi calreticulin. Mol. Immunol. 47, 1516–1521. https://doi.org/10.1016/j.molimm.2010.01.019.
van Gunsteren, W.F., Billeter, S.R., Eising, A.A., Philippe, H., Hünenberger, P., Krüger, P., Mark, A.E., Scott, W.R.P., Tironi, I.G., 1996. Biomolecular Simulation: The GROMOS96 Manual and User Guide 86 Vdf Hochschulverlag AG an der ETH Zürich.
van Schaarenburg, R.A., Suurmond, J., Habets, K.L.L., Brouwer, M.C., Wouters, D., Kurreeman, F.A.S., Huizinga, T.W.J., Toes, R.E.M., Trouw, L.A., 2016. The production and secretion of complement component C1q by human mast cells. Mol. Immunol. 78, 164–170. https://doi.org/10.1016/j.molimm.2016.09.001.
van Tong, H., Brindley, P.J., Meyer, C.G., Velavan, T.P., 2017. Parasite Infection, Carcinogenesis and Human Malignancy. EBioMedicine 15, 12–23. https://doi.org/10.1016/j.ebiom.2016.11.034.
Wallis, R., Shaw, J.M., Uitdehaag, J., Chen, C.B., Torgersen, D., Drickamer, K., 2004. Localization of the serine protease-binding sites in the collagen-like domain of mannose-binding protein: Indirect effects of naturally occurring mutations on protease binding and activation. J. Biol. Chem. 279 (14), 14065–14073. https://doi.org/10.1074/jbc.M400171200.
Wang, J., Wolf, R.M., Caldwell, J.W., Kollman, P.A., Case, D.A., 2004. Development and testing of a general amber force field. J. Comput. Chem. 25, 1157–1174. https://doi.org/10.1002/jcc.20035.
Weinberger, K., Collazo, N., Aguillón, J.C., Molina, M.C., Rosas, C., Peña, J., Pizarro, J., Maldonado, I., Cattan, P.E., Apt, W., Ferreira, A., 2017. Triatoma infestans Calreticulin: Gene Cloning and Expression of a Main Domain That Interacts with the Host Complement System. Am. J. Trop. Med. Hyg. 96, 295–303. https://doi.org/10.4269/ajtmh.16-0642.
Wijeyesakere, S.J., Rizvi, S.M., Raghavan, M., 2013. Glycan-dependent and -independent interactions contribute to cellular substrate recruitment by calreticulin. J. Biol. Chem. 288, 35104–35116. https://doi.org/10.1074/jbc.M113.507921.
World Health Organization, 2015. Chagas disease in Latin America: an epidemiological update based on 2010 estimates. World Health Organ. Wkly. Epidemiol. Rec. 6, 33–44.
Xiao, F., Wei, Y., Yang, L., Zhao, X., Tian, L., Ding, Z., Yuan, S., Lou, Y., Liu, F., Wen, Y., Li, J., Deng, H., Kang, B., Mao, Y., Lei, S., He, Q., Su, J., Lu, Y., Niu, T., Hou, J., Huang, M.J., 2002. A gene therapy for cancer based on the angiogenesis inhibitor, vasostatin. Gene Ther. 9, 1207–1213. https://doi.org/10.1038/sj.gt.3301788.
Yoshida, N., 2009. Molecular mechanisms of Trypanosoma cruzi infection by oral route. Mem. Inst. Oswaldo Cruz 104 Suppl, 101–107. https://doi.org/10.1590/S0074-02762009000900015.
Zhou, H., Zhou, Y., 2002. Distance-scaled, finite ideal-gas reference state improves structure-derived potentials of mean force for structure selection and stability prediction. Protein Sci. 11, 2714–2726. https://doi.org/10.1110/ps.0217002.
Zenina, A.V., Kravtsov, E.G., Tsetsegsaikhan, B., Yashina, N.V., Dalin, M.V., Karpenko, L.P., Sheklakova, L.A., Kallinikova, V.D., 2008. The study of immunological component in antitumor effect of *Trypanosoma cruzi*. Bull. Exp. Biol. Med. 145 (3), 352–354. https://doi.org/10.1007/s10517-008-0089-3.
Zúñiga, J., Fuenzalida, M., Guerrero, A., Illanes, J., Dabancens, A., Díaz, E., Lemus, D., 2003. Effects of steroidal and non steroidal drugs on the neovascularization response induced by tumoral TA3 supernatant on CAM from chick embryo. Biol. Res. 36, 233–240.